

Experimental Investigation of Performance of a Small Scale Horizontal Axis Wind Turbine Rotor Blade

R. Supreeth^{*‡}, A. Arokkiaswamy^{**}, Nagarjun J. Raikar^{***}, H. P. Prajwal^{***}

^{*} Research Scholar, Department of Aeronautical Engineering, Dayananda Sagar College of Engineering, Assistant Professor, Department of Aerospace Engg, Rashtreeya Vidyalaya College of Engineering, Bengaluru-560059, India

^{**} Professor and Head, Department of Aeronautical Engineering, Dayananda Sagar College of Engineering, Bengaluru 560078, India

^{***} Department of Aerospace Engineering, Final Year Students, Rashtreeya Vidyalaya College of Engineering, Bengaluru 560059, India

(supreeth@rvce.edu.in, Swamy.aroks@gmail.com, nagarjunjr.ae15@rvce.edu.in, prajwalhp.ae15@rvce.edu.in)

[‡] Corresponding Author; R Supreeth, Assistant Professor, Department of Aerospace Engineering, Rashtreeya Vidyalaya College of Engineering, R V Vidyanikethan Post, Mysore Road, Bengaluru-560059, Karnataka, India. Off-+91-080-67178406, supreeth@rvce.edu.in

Received: 21.08.2019 Accepted: 18.10.2019

Abstract- Analytically and experimentally evaluating the performance of a 2kW small scale horizontal axis wind turbine rotor blade has been presented by the authors. Initially, the performance of linearized blade is predicted theoretically at wind velocities ranging from $V=1-20\text{m/s}$ and $\text{TSR}=1-20$. Further, appropriate scaling laws have been incorporated to scale down the original blade and subsequently its performance is appraised at the design conditions. Vital research outcomes suggests that by incorporating suitable scaling laws the performance of the downsized rotor blade can precisely be determined which is comparable with the actual blade. Finally, the research concludes that the non-consideration of hub losses, 3-Dimensional flow effects and unsteady aerodynamic effects will certainly cause the experimental results to slightly be lower than the BEM theory.

Keywords: Blade Element Momentum Theory, Coefficient of Power, Renewable Energy, Rotor Blade Scaling, Wind Energy

1. Introduction

In order to alleviate and mitigate the effects of climate change, tremendous amount of research has been focused towards embracing non-conventional renewable sources for energy generation [1]. Energy demands of the progressive era can be fulfilled by adopting biomass, hydro, geothermal, solar, wind, wave, and tidal energy [1]. Among them, wind energy is the oldest form of energy ever utilized by mankind. Long association with humanity and the time tested developments in the field of wind energy has propelled wind turbines as the ideal replacement for fossilized fuels [2]. In addition, advancements in the field of material development [3], power electronics [4], computational analysis, vibration control etc. has enthusiastically widened the scope for efficiently extracting energy from the wind. Additionally, the favorable policies initiated by governmental agencies have

further catalyzed the interest in embracing wind turbine technology [5]. Widespread extraction of energy through wind began in the early 1990s during which a modest contribution of 1GW was witnessed. Later, the global cumulative installed wind power capacity steadily increased to 200GW by 2010 and at the end of 2017 a massive 539GW of global installed capacity was registered. Around 20% of global energy generated in 2018 was contributed solely by wind energy and it is surmised that by 2030 around 30% of the global energy needs will likely to be satisfied by wind turbines alone [6]. Currently, only large scale wind turbines have been the frontrunners in the field of wind energy and largely been contributing towards global energy needs. However, most of the wind turbines available today are extremely large and are usually coupled with astronomical costs due to which a large section of population residing

away from the grid have deliberately been disconnected and eventually dwarfed their socio-economic development [7] [8]. Hence, to fulfill the demands, a recent focus has been shifted towards the development of small-scale wind turbines (SSWTs) which are ideal solution for off-the-grid power generation [8]. Innovative contributions in the field of battery technology [9], accurate weather forecasting [10] have further motivated substantial efforts in building an efficient and effective small scale wind turbine system [11].

Efforts made by Singh et al. [12] in altering the trailing edge thickness has proved to be beneficial in improving the aerodynamic characteristics of the airfoil for wind turbine blades. S823 and S822 airfoils designed by Somers [13] renders optimum aerodynamic and structural prerequisites to the blade especially while operating at low Reynolds number flows. Prasad et al. [14] numerically presented that thickening the airfoil by 30% would revamp the aerodynamic efficiency in comparison with the baseline model. Experimentally, Göçmen et al. [15] proved that by modifying the upper surface of the airfoil the aerodynamic behavior can significantly be enhanced. Suitability of Eppler and XFOIL software for numerical testing of aerodynamic behavior of airfoils have been demonstrated by Somers et al. [16] and also validated with experimental data. As shown by Haibo Jiang et al. [17] a wind turbine projects a maximum coefficient of power when λ approaches infinity and is unlikely to outperform Betz limit under the absence of all losses. Gur et al. [18] proposed the importance of incorporating the influence of drag coefficient and tip losses for simulating real world environment. Lin Wang et al. [19] demonstrated the adoption of design wind speed $U_{design}=8\text{m/s}$ and tip speed ratio around $\lambda=5-6$ to achieve optimum performance for annual wind speeds varying between 5 m/s and 6m/s. Experiments performed by Giguère et al. [20] highlighted the provision of linear taper and nonlinear twist to be beneficial in maximizing the annual energy production of the wind turbine. Through BEM theory, Pathike et al. [21] developed a novel blade for operation at velocity 3-7 m/sec. The blade was effective in generating a decent power of 235W at the selected geometrical and flow conditions. Tests carried out by Collecutt et al. [22] conveyed that operating a wind turbine at non-optimized state will result in performance deterioration to the tune of 10%. Manoj Kumar Chaudhary et al. [23] proposed the significance of pitch angle and tip speed ratio on performance of the blade. Simplicity of implementing Qblade software for design and optimization of the blades for low speed micro wind turbines have been reported by Drumheller et al. [24]. Bayati et al. [25] articulated the methodology for assessing the performance of the scaled down wind turbine models. Treuren et al. [26] discussed the scaling and testing of the SSWTs in a wind tunnel. By performing experimental testing, Treuren et al. [27] suggested the importance of retaining TSR, blade material, geometry, number of blades and Reynolds number in carrying out scaled-down testing. Experimental outcomes of Bottasso et al. [28] on down sized wind turbine models showed that higher C_p can be achieved when the TSR is maintained between 7 and 8.

The current project involves the design, development and experimental testing of blades for 2kW small scale horizontal axis wind turbines. Traditional Blade Element Momentum theory (BEMT) will be utilized to arrive at a geometrically feasible rotor blade suiting the requirements. Analytically, the coefficient of performance C_p of the blade will be deduced through BEM equations for a range of velocities V and tip speed ratios λ . Scaling laws will be applied to downsize and fabricate the model to be retrofitted to an existing wind turbine generator. Finally, the performance of the scaled-down blade will experimentally be assessed for the given flow conditions and compared with the BEM outcomes.

2. Blade Element Momentum Theory

Traditionally, BEMT theory is implemented for design of rotor blades for wind turbines irrespective of the scale of operation. BEM theory has been dedicatedly developed by blending momentum theory and blade element theory, known as strip theory. Strip theory, segments the rotor blade into N number of small elements and the performance of the entire rotor blade can be appraised by summing the performance of each blade segment.

2.1. Momentum Theory

Based on BEM theory, the total thrust forces generated on the blade can be estimated by applying linear momentum conservation to the control volume as in fig.1.

$$T = \frac{1}{2} \rho A_2 (U_1^2 - U_4^2) \quad (1)$$

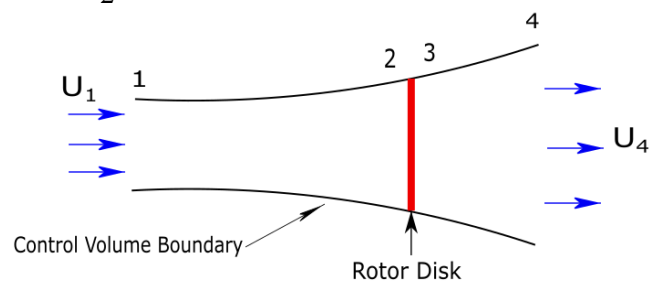


Fig. 1. Control volume approach for a wind turbine rotor disk

The fractional decrease in the wind velocity as it reaches the rotor plane is termed as the Axial Induction Factor a and represented as

$$a = \frac{U_1 - U_2}{U_1} \quad (2)$$

Power from the wind in terms of axial induction factor is given by

$$P = \frac{1}{2} \rho A U^3 4a(1 - a^2) \quad (3)$$

Power Coefficients C_p and thrust coefficients C_T for the rotor blade are defined by the equations (4) and (5)

$$C_p = 4a(1-a)^2 \quad (4)$$

$$C_T = \frac{T}{\frac{1}{2}\rho U^2 A} \quad (5)$$

To simulate the real working environment of a rotor blade, wake rotation behind the rotor has to be included in the BEM theory. The generation of angular momentum in the wake utilizes the energy from the rotor blade, therefore resulting in lower power output. The drop in the angular momentum is given by angular induction factor a' . The wake downstream a real rotor blade is displayed in fig.2.

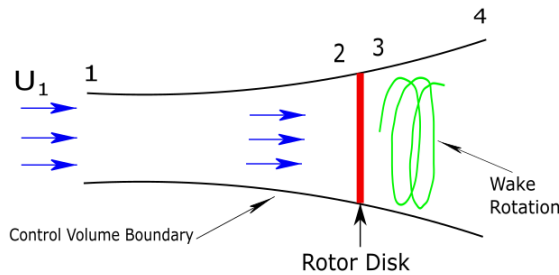


Fig. 2. Representative sketch for a wind turbine model with downstream wake rotation

Thrust in terms of a and a' acting on the annular element is given by

$$dT = 4a'(1+a')\frac{1}{2}\rho\Omega^2 r^2 2\pi dr \quad (6)$$

Next, by including the axial induction factor a and free stream velocity U , the equation for thrust can be

$$dT = 4a(1-a')\frac{1}{2}\rho U^2 2\pi dr \quad (7)$$

Equating the above two expressions for an annular element, we get

$$\lambda = \frac{\Omega R}{U} \quad (8)$$

Now, by applying the angular momentum conservation, the torque developed by an annular element of the blade is imparted by the expression

$$dQ = 4a'(1-a')\frac{1}{2}\rho U \Omega r^2 2\pi dr \quad (9)$$

The power contrived by each element of the blade is

$$dP = \frac{1}{2}\rho A U^3 \left[\frac{8}{\lambda^2} a'(1-a)\lambda_r^3 d\lambda_r \right] \quad (10)$$

The incremental power coefficient dC_p contributed by each annular element is

$$dC_p = \frac{dP}{\frac{1}{2}\rho A U^3} \quad (11)$$

At last,

$$C_p = \frac{8}{\lambda^2} \int_0^\lambda a'(1-a)\lambda_r^3 d\lambda_r \quad (12)$$

The power produced by an actual rotor blade is always low compared to the ideal blade. The same is outlined in fig.3.

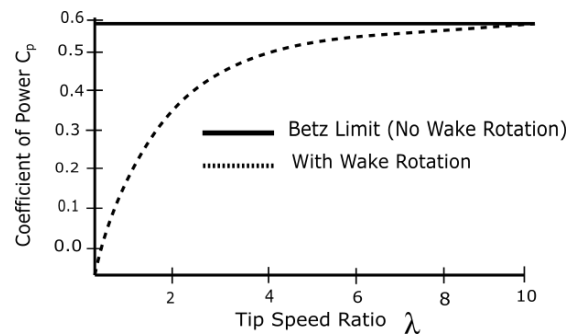


Fig. 3. C_p trend for blade with and without wake rotation

2.2 Blade Element Theory

In the Blade element theory, the rotor blade is equally segregated into N elements as given in fig.4. The forces on each element are calculated using the formulae by contemplating the lift and drag forces acting on the individual elements of the blade as given in fig.5.

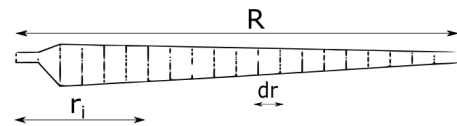


Fig. 4. Schematic of a rotor blade

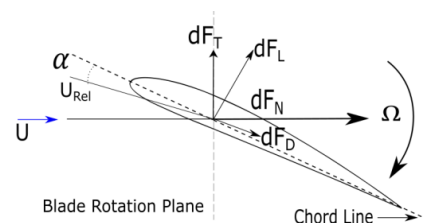


Fig. 5. Primary forces acting on the blade element

From the geometry, the following relations can be derived.

$$\varphi = \theta_p + \alpha_r \quad (13)$$

$$\tan\phi = \frac{1-a}{(1+a')\lambda_r} \tag{14}$$

$$U_{rel} = \frac{U(1-a)}{\sin\phi_r} \tag{15}$$

$$dF_L = \frac{1}{2} \rho U_{rel}^2 C_l c dr \tag{16}$$

$$dF_D = \frac{1}{2} \rho U_{rel}^2 C_d c dr \tag{17}$$

$$dF_N = dF_L \cos\phi + dF_D \sin\phi \tag{18}$$

$$dF_T = dF_L \sin\phi - dF_D \cos\phi \tag{19}$$

For finite number of blades B , the normal force dF_N and torque dQ occurring at a distance, r , from the axis of rotation are derived by combining the previous equations.

$$dF_N = B \frac{1}{2} \rho U_{rel}^2 (C_l \cos\phi + C_d \sin\phi) c dr \tag{20}$$

$$dQ = B \frac{1}{2} \rho U_{rel}^2 (C_l \sin\phi - C_d \cos\phi) c r dr \tag{21}$$

The detailed step wise procedure of BEMT employed for predicting the behavior of the rotor blade is illustrated in fig.6.

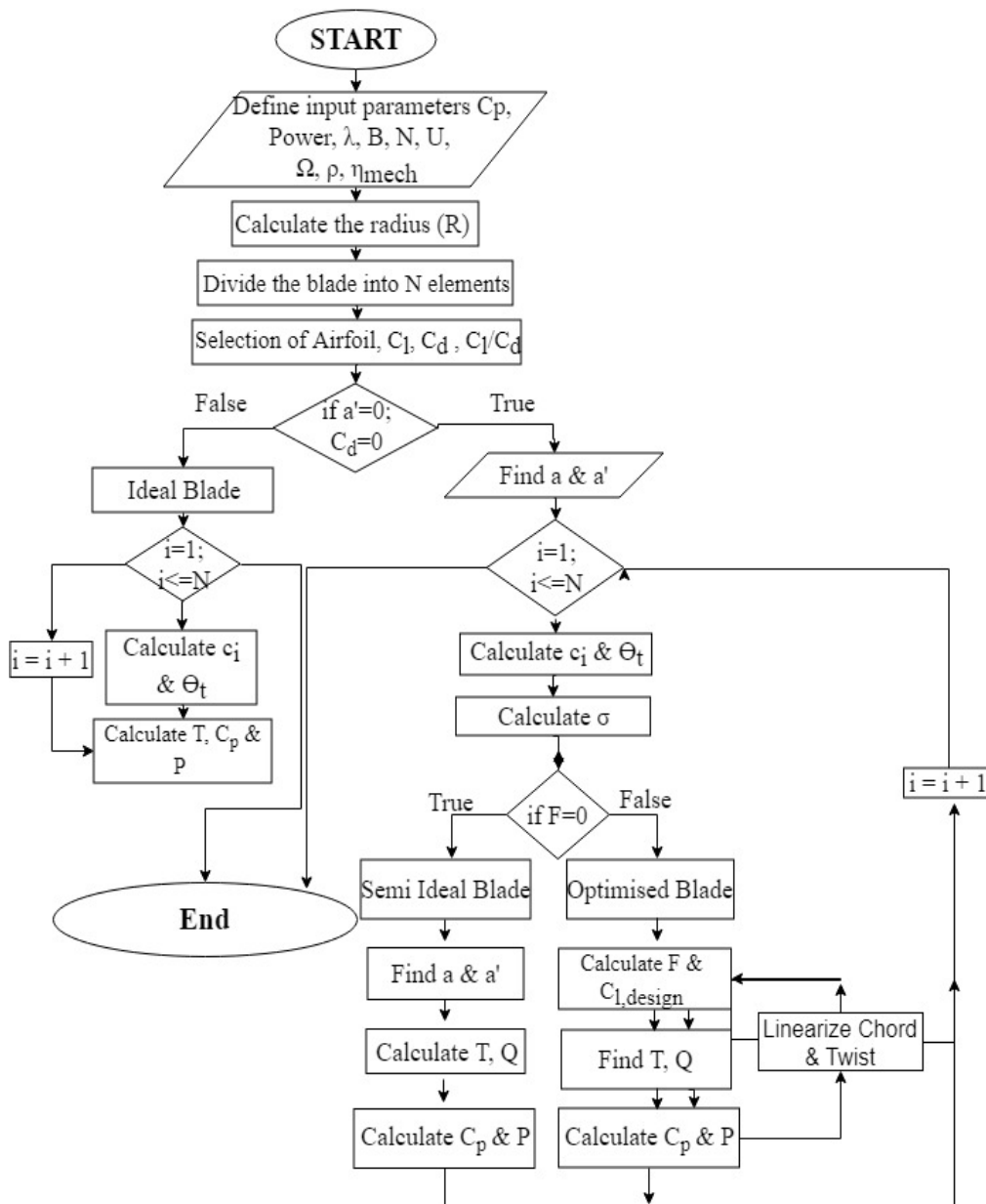


Fig. 6. Flow Chart of BEM theory

3. Wind Turbine Specifications

The detailed technical and operating conditions are briefly specified and tabulated in table 1.

Table 1. Detailed specifications of the wind turbine under consideration

Type	Horizontal axis-Upwind	Hub radius (R_b)	0.1 m
Rated Power (P)	2kW	Number of blades (B)	3
Design wind speed (V)	10m/s	Design tip speed ratio (λ)	7
Rotor Radius (R)	1.6 m	Airfoils Used	S823 (Root: 0-30%)
Rotor Diameter (D)	3.4 m		S822 (Primary: 30%-Tip)

4. Geometrical Design and Performance of Rotor Blade- BEM Methodology

BEM theory has been employed to develop blade geometry for a 2kW horizontal axis wind turbine. By sequentially applying BEM principles, geometrically dissimilar derivatives of the blade will be yielded as illustrated in the flow chart and the same is explained in the ensuing sections.

The geometrical profile of a rotor blade is specified majorly by the chord c_i and twist θ_{Ti} distribution as constituted in fig.7a and 7b. As stated previously, BEM theory works iteratively in predicting the geometry of the blade. Initially in the BEM sequence, the wake rotation ω , drag coefficient C_d and tip losses F are ignored leading to an idealized blade as highlighted in fig.7a and 7b. The idealized blade displays a maximal chord $c_i=0.492m$ at $r_i=0.05R$ which then tapers off to $c_i=0.066m$ at the tip where $r_i=1R$. Alongside, the idealized blade exposes an utmost twist angle $\theta_{Ti}=56.265^\circ$ at $r_i=0.05R$ that untwists itself to 0° at $r_i=1R$. Succeeding to it, the consideration of wake rotation ω , drag

coefficient C_d and tip losses F influences the geometry of the blade and remodels the chord c_i and twist θ_{Ti} distribution resulting in an optimized blade as highlighted in the figures. The optimized blade exhibits $c_i=0.22m$ and $\theta_{Ti}=40.97^\circ$ at $r_i=0.05R$ and then recedes to least value of $c_i=0.065m$ and $\theta_{Ti}=0^\circ$ at $r_i=1R$. Figures clearly manifest the reduction in the chord c_i and twist θ_{Ti} distribution of the optimized blade in relation to the idealized blade. Despite this reduction, the geometrical distribution of the optimized blade is deemed complex due to the presence of abrupt changes in chord and twist mostly across the root section. Precipitous change in blade geometry imposes severe manufacturing complexities and invites special techniques that can rarely be achieved using any off-the-shelf techniques [29]. Producing a blade via any non-conventional processes will eventually accelerate the cost of the blade [30]. To avoid this, and as a general practice, the chord c_i and twist θ_{Ti} distribution of the optimized blade will ultimately be linearized rendering a smooth as well as simple geometrical distribution that eases the manufacturing ability of the blade. The chord c_i and twist θ_{Ti} of the linearized blade bestowed in fig.7a and 7b is juxtaposed with the idealized and optimized blades.

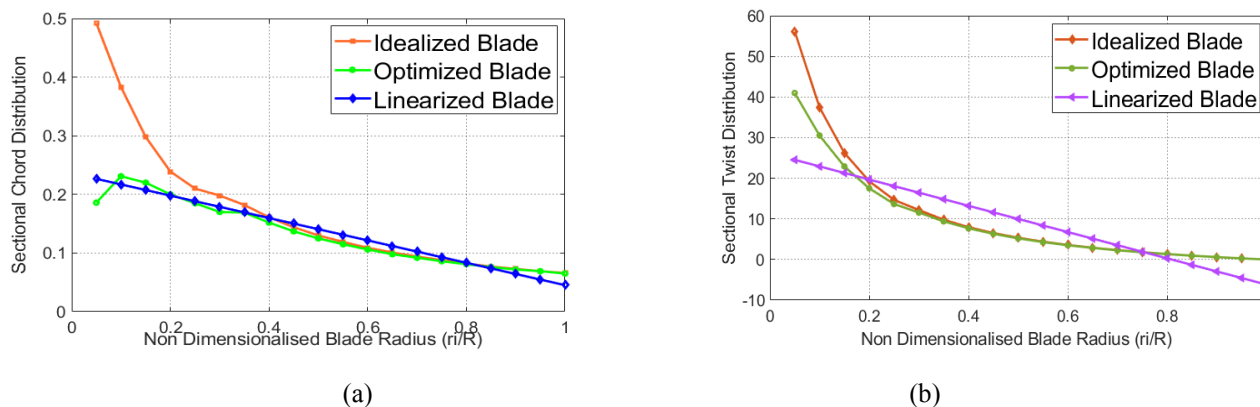


Fig. 7. Chord and Twist distribution of the blades predicted by BEM theory

Solidity is a crucial performance parameter tightly intertwined with the chord c_i distribution of the blade and is defined as the ratio of the blade planform area to the projected swept area and given as $\sigma' = Bc / 2\pi r$. The expression clearly exemplifies that for achieving high rotational RPMs, the blade area should necessarily be maintained as low as possible with optimum structural strength. The variation in the solidity of the idealized, optimized and linearized blades is projected in fig.8. Visually it is evident that as the idealized blade predicts large values of chord distribution c_i , solidity will invariably be the highest

among all the blades. Since, the blade root endures all the aerodynamic and structural loads arised during operation, the root section will naturally expose large area and the solidity irrespective of the blade will be more at the root section. This is true even in our case where the blades exhibit their highest solidity only between $0.05R$ to $0.3R$ and later the solidity tapers off gradually. Beyond $0.3R$, all the blades display a solidity trend that almost coincides with each other. The average solidity for the idealized blade measured $\sigma=0.3122$ as compared with $\sigma=0.2127$ and $\sigma=0.1953$ of optimized and linearized blades respectively.

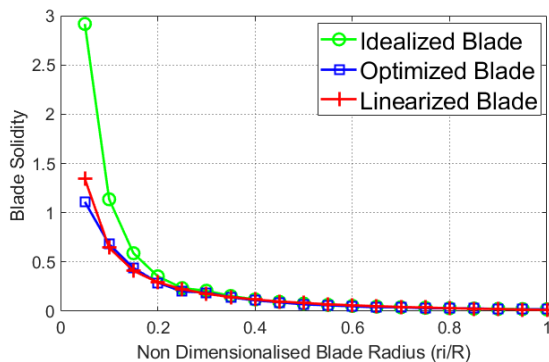


Fig. 8. Local solidity distribution for idealized, optimized and linearized blades

Power developed by the wind turbine rotor blade is mathematically expressed as $P = \frac{1}{2} \rho \pi R^2 U^3 C_p \eta$. From the equation it is seen that power varies with cube of velocity. The power with respect to the wind velocity of all the blades is provided in fig.9a. It is visually evident from the figure that the power generated by all the blades is less at low wind

speeds. But, this tendency dramatically changes as the velocity increases. Equivalently, the coefficient of power C_p of all four blades is compared in 9b. As idealized blade functions close to the Betz limit, C_p is at the top with $C_p=0.589$ and later preceded by $C_p=0.47256$, $C_p=0.4155$ and $C_p=0.4095$ of the semi idealized, optimized and linearized blades.

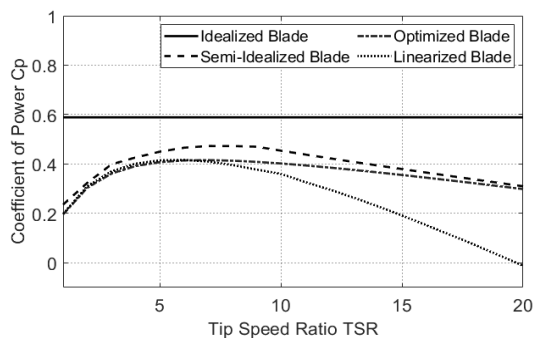
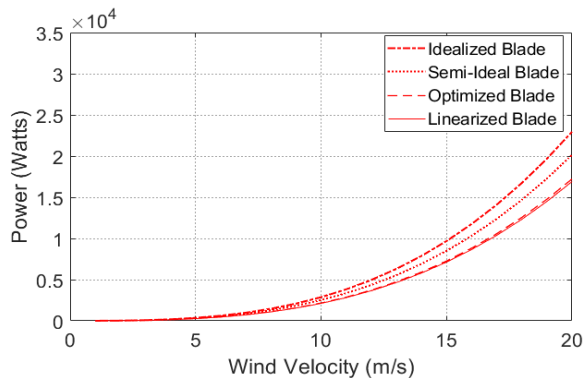


Fig. 9. Comparison of Power and Coefficient of Power C_p for all the blades

5. Scaling of the Rotor Blade

Since most wind turbines are enormously sized, creating a facility to accommodate full scale wind turbine would be logistically cumbersome. Besides, a full scale test of a wind turbine would bring about astronomical costs that escalate the total production cost of the turbine. Nevertheless, the performance of a wind turbine can be verified experimentally by downsizing. Scaling down the wind turbine allows one to conduct the tests in a much smaller facility while still

obtaining the vital aerodynamic results with a respectable accuracy if done correctly. In this research work, the scaling laws are applied as reported in [21-22]. Following a similar analogy, to suit our specification, the radius of the blade is scaled-down by a factor $f=2.4263$. Subsequently, all the other critical parameters such as wind velocity, TSR, Reynolds number are correspondingly conserved as per the scaling laws. The scaling factors for the underlying research work are listed in table 2.

Table 2: Scaling parameters incorporated in the design of the scaled-down model

Sl. No	Scaling Parameter	Symbol	Scaling Factor	Original Value	Scaled-down Value
1	Blade Radius	R	f	1.608 m	0.663 m
2	Chord Max	C_{max}	f	0.186 m	0.0766 m
3	Chord Min	C_{min}	f	0.0455 m	0.018 m
4	Rotational Velocity	Ω	1/f	43.43 rad/s	105.36 rad/s
5	Rotor Power	P	f^2	2000 W	854 W

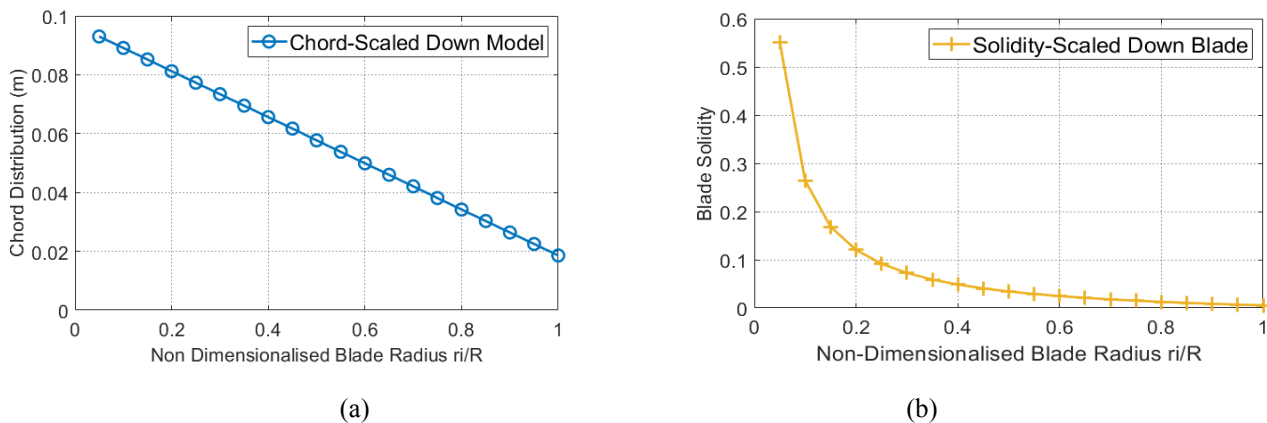


Fig. 10. Chord and solidity distribution of the scaled-down model-BEM Method

Based on the scaling philosophy, chord of the linearized blade is downsized suitably and the same is provided in fig.10. The chord of the linearized blade has been geometrically scaled-down by a factor 2.4263 suiting the experimental set-up restrictions. Post scaling, the maximum and minimum chord $c_{max}=0.093$ and $c_{min}=0.0186$ has been

measured at $r_i=0.05R$ and $r_i=1R$ respectively. Corresponding to the chord, the solidity of the scaled-down blade is manifested in fig.10b. Indistinguishable to the linearized blade, the peak local solidity of the scaled-down blade is reported to be $\sigma'=0.5515$ at $r_i=0.05R$. The total solidity of the downsized blade is found to be $\sigma=0.0802$.

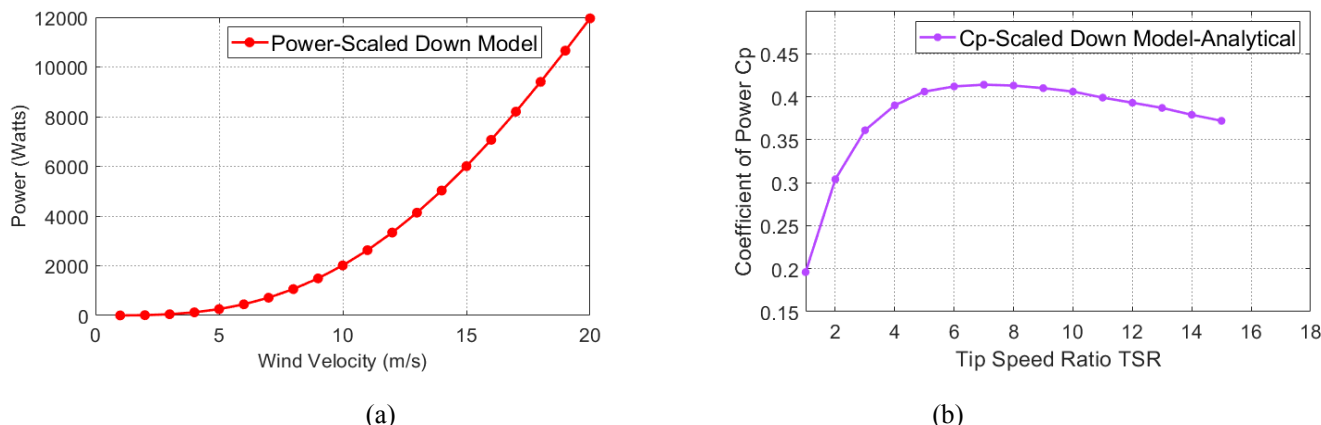


Fig. 11. Power P and Coefficient of Power C_p of the scaled-down model-BEM Method

The power P and coefficient of power C_p of the scaled-down model are illustrated in fig.11. The power developed by the original linearized blade is found to be $P=2149.9$ Watts

at design velocity and the equivalent coefficient of power C_p is 0.4143 at design TSR. By comparison, the power and C_p of the scaled-down blade are found to be promising.

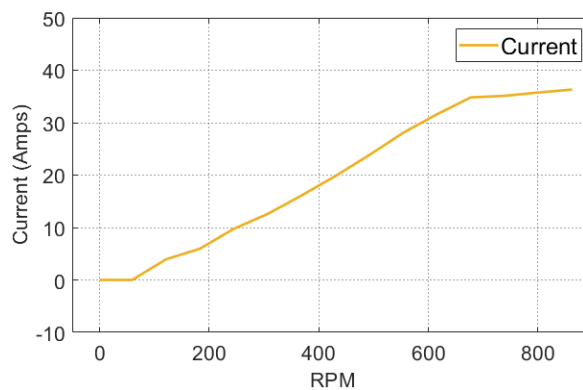
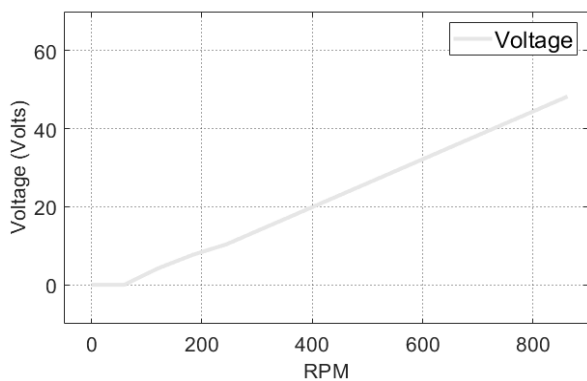


Fig. 12. (a) Blower Facility (b) Wind Turbine Test Rig (c) Control Panel

6. Experimental Methodology

The power output of the duly fabricated scaled-down rotor blade has been tested at an in-house wind turbine test rig. The test rig is a 3 bladed upwind rotor configuration with blower duct and control facility as shown in fig.12. The experimental set-up is installed with a 1.5m diameter blower facility driven by a variable speed 20hp motor and capable of producing a maximum wind velocity of 20m/s at peak RPM. The freestream velocity at different stations from the blower exit was ascertained through a vane anemometer. Prior to the utilization, its calibration was confirmed by recording different wind velocities in a low speed wind tunnel and eventually the anemometer was found to be performing with accuracy more than 99%. Further, with the aid of the anemometer, the turbulence intensity of the blower facility

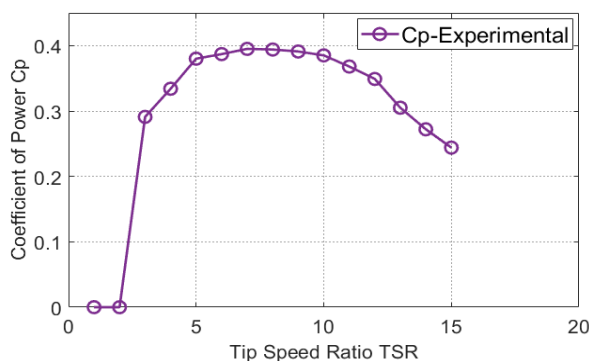
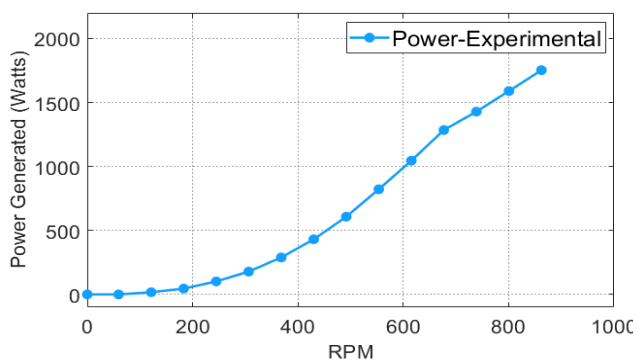
was recorded and found to be less than 2% across various radial planes from the exit of the facility. Upstream to the blower, a 1kW wind turbine generator is mounted on a railing platform which facilitates the movement of the generator longitudinally back and forth. Depending on the need, the generator can be positioned and held rigidly at any distance from the blower. The test rig is incorporated with a direct drive generator with a rated power of 1.5kW at 10m/s and 500 RPM. Next, Equinox optical tachometer with a range of 5-30V DC, 300mA was equipped to determine the turbine rotational speed. The generator is interfaced to a high speed controller, battery system and an inverter. An AC voltmeter and AC ammeter connected to the circuit measured the voltage and current at respective wind velocities. Finally, the power developed by the turbine at given wind velocity is determined using simple power equation $P=V*I$.



(a) (b)
Fig. 13. Experimental Voltage and Current at varying velocity

The objective of determining the power output of the scaled turbine depends on the voltage and current measurements at different wind velocities. Based on wind velocity and corresponding RPM, the voltage V and proportional current I produced is shown in figure13. Later the whole experiment of measuring the voltage and current

was repeated from 1-15m/s and again from 15-1m/s to verify the repeatability of the test results and it was found to be more than satisfactory as the repeatability tests exhibited the same values of measurements consistently at a given wind velocity.



(a) (b)
Fig. 14. Power P and Coefficient of Power C_p of the scaled-down model-Experimental Method

The experimental power output of the scaled-down blade is charted in fig.14a. In the research work, as defined earlier a scaling factor of 2.4263 has been introduced. To comply with the scaling laws the wind velocity was to be increased by 2.4263 times the free stream velocity. Accordingly, the initial wind velocity begins at $V=2.4263m/s$ and goes up to

$V=48.56m/s$ with a design velocity projected at $V_{design}=24.263m/s$. But, the maximum wind capacity of the blower is limited to $V=20m/s$. Due to this limitation and also considering the RPM capacity of the generator, the power yielded by the scaled-down model was established at RPM corresponding to velocity ranging from $V=1-15m/s$ and the

same has been plotted. This figure will seldom be used for evaluation. For sensible comparison, the coefficient of power C_p for the scaled-down version has been estimated as a ratio of power output of the scaled model to the power output of the actual model. This conversion dispensed a promising

trend as same as the prototype and presented in fig.15b. Eventually, the coefficient of power C_p of the scaled model evaluated through iterative and experimental schemes are compared in fig.15.

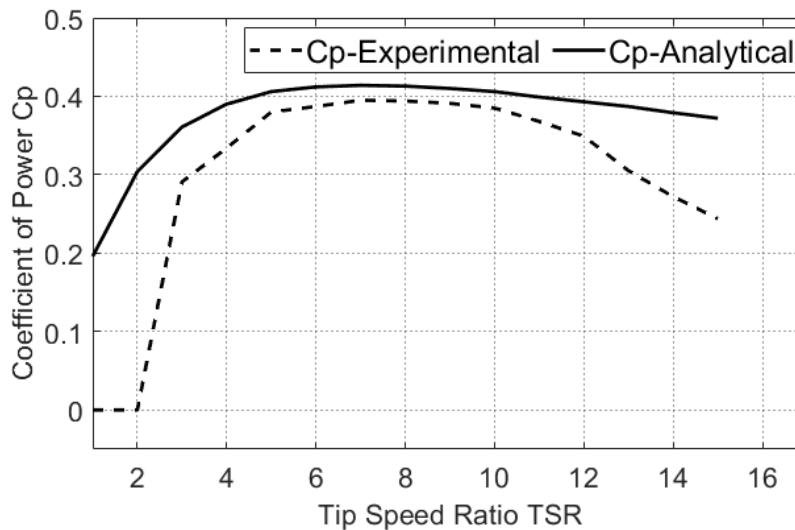


Fig. 15. Comparison of Analytical and Experimental C_p of the scaled-down model

7. Results & Discussions

Section 4 essentially deals with the geometrical description of the blades and their performance contrived through BEM theory. Figure 7a and 7b exemplifies the radial distribution of chord and twist geometry in regards to the idealized, optimized and linearized blades. BEM theory automatically predicts a geometry that satisfies the aerodynamic as well as the structural requirements of the blade. The geometry renders a root that is sufficiently large in order to handle the loads encountered during blade operation. Similarly, the blade equally exhibits a tapering slender geometry that is potential enough to generate high aerodynamic forces coupled with least drag forces. Undoubtedly, in the figures, the chord and twist profiles of the ideal blade are comparatively higher. This is because, initially BEM theory neglects the consequential repercussions of wake ω , drag C_d and tip losses F on the blade geometry. Power generated by any rotor blade will clearly be higher due to the absence of all the detrimental effects causing reduction in power. Correspondingly, while operating ideally, BEM theory estimates reasonably higher values of chord and twist distribution corresponding to the largest power output from the blade sections. But, the chord and twist distribution certainly reduces when the practical effects of wake, drag and tip losses are encompassed. The optimized blade resulting from the consideration of wake, drag and tip losses exhibit a blade geometry that is comparatively simpler than the idealized blade. Finally, the blade geometry is linearized to simplify manufacturing.

Since the blade geometrical distribution is inevitably linked to solidity, the solidity of the idealized blade will undisputedly be the highest followed by the optimized and the linearized blades. Blades with higher solidity exhibits

better structural properties while low solidity renders slender blades with higher aerodynamic output. The variation in the local solidity with radius of the blades is outlined in fig.8. The mean solidity recorded for the ideal blade is $\sigma=0.3122$ in comparison with the optimized blade that exhibited a mean solidity of $\sigma=0.2127$. Similarly, the linearized blade with simple geometry portrayed the least solidity equaling $\sigma=0.1953$. From the comparison we understand that the idealized blade demonstrated a mean solidity which is 31.8% and 37.4% higher than the optimized and the linearized blades. High solidity blades with large concentration of blade geometry are more suited for mechanical wind turbines requiring high torque. On contrary, for power generating wind turbine machines, the solidity needs to be maintained low in order to produce high RPM rather than high torque. Hence, for electrical wind turbine, the optimum solidity can be realized by simplifying the chord and twist distributions through linearization and that may also prove advantageous in terms of better TSR, power coefficients C_p and many more.

The power output of each blade is conceived in fig.9a. A parabolic increase in the power can be witnessed across all the blades particularly when the wind speed transcends the design speed at $V=10m/s$. With the increase in wind velocity all the blades exhibited the same nature. Comparatively, the power output of the idealized blade is high across all the velocities considered. Wake is a prominent factor affecting the torque and thus the power output of the rotor blade. Disregarding wake in the design of an idealized blade always renders highest power output at all velocities and the same is disclosed in the figure. Power curve of the idealized blade is seen at the top, followed by the semi idealized, optimized and lastly by linearized blade. When the velocity reaches design condition, the theoretical mechanical power of the

blades measured were 3287W, 2518.21W, 2151.98W and 2112.45W respectively. Comparatively, the semi idealized, optimized and linearized blades produce 12.2%, 24.98% and 35.7% less power output at V_{design} . Reduction in power is mainly due to wake and drag in semi idealized case and wake, drag and tip losses in the optimized and linearized cases. Though, semi idealized and optimized blades exhibit a notable reduction in power when compared to the idealized blade, the percentage change in power between the optimized and linearized blade is just 1.8%. The investigation shows that the idealized and semi idealized blades produce remarkable power only under hypothetical contexts. Incorporating the apparent effects of wake and drag will certainly reduce the power of the idealized and semi idealized blades by huge margin. A blade subjected to an actual working environment will yield power akin to the optimized blade in our case. With the backdrop of all the blades, invariably only the optimized blade is realizable and the power exhibited is more or less achieved in the actual environment. Collating the power output of the linearized blade with optimized blade, the percentage difference in power reduction is just 1.83%. Since linearization reduces the power output of the optimized blade only by a meagre margin, the trade-off provided in terms of manufacturing cost reductions will hugely be favorable. Moreover, the optimized blade will perform optimally only at ON-design conditions and this will necessarily not guarantee the same performance at OFF-design conditions and the geometry will no more be optimal. Hence, linearization provides obvious advantageous aspects to the wind turbine manufacturers with a meagre sacrifice in power output. Relevant to the power output P , the equivalent power coefficient C_p of all the blades are compared in fig.9b.

Section 5 deals with the geometric and performance assessment for the scaled-down model through BEM theory. In the research work elucidated, the geometrical scaling has been arrived based on the maximum diameter of the blower which is around $\phi=1.5m$. On the other hand, the diameter of the full scale blade determined through BEM analysis is found to be $\phi=3.6m$ including the hub diameter. To retrofit the blade in the available equipment, a geometric scaling factor of $f=2.4263$ is required which allows the blade to be accommodated conveniently within the effective downstream wake of the blower. Using the scaling factor, the radius and the chord distribution of the blade has been downsized by 2.4263 times the original dimension and the same are presented in fig.10a and 10b. Also, the performance of the scaled-down blade is assessed through the same BEM fundamentals applied for the actual blade. Adhering to the dynamic similarity rule, the TSR and the wind velocity V are proportionately upsized by 2.4263 times. For the latest values of TSR and V , the power and C_p for the scaled-down blade is depicted in figure 11 and are found to be totally tallying with the actual blade values.

Section 6 elucidates the performance of the scaled-down model realized through experiments. Figure 13a and 13b portrays the generator voltage V and current I values gauged at different RPM of the turbine. In fig.13a it can be observed that the voltage generated in the circuit is zero during the

initial stages of turbine RPM. The voltage is zero for the first two RPM suggesting that the turbine has not cut-in and hasn't produced any useful torque for generating power. But, the drift in voltage starts to rise as soon as the turbine RPM surpasses an RPM corresponding to a wind velocity of $V=3m/s$. This shows that there is a potential difference created only when the turbine reaches $\Omega=121$ RPM at $3m/s$. Beyond this mark, there is a steady increment in the voltage across the circuit illustrating a constant slope voltage with rise in the wind velocity and relevant RPM. The voltmeter records a maximum voltage of 48.23 volts at $\Omega=862$ RPM when the wind velocity reaches $15m/s$. The proportional current recorded is highlighted in fig.13b. The figure puts up a similar trend of 0 amperes at initial RPM due to the non-generation of power prior to cut-in velocity. Once the RPM passes the cut-in velocity at $3m/s$ the current starts flowing in the circuit and the incremental current measured is emphasized in the figure. With increase in RPM the current increase linearly. Nonetheless, the rising curve manifests a saturation point as the RPM negotiates $12m/s$ corresponding to $\Omega=730$ RPM. Post 730RPM, the slope of the curve becomes sluggish without any extra increase in the current before showing signs of saturation farther 730RPM signifying that the generator is functioning at its full peak capacity. The corresponding power generated by the scaled-down blade is determined by considering the product of voltage and current at various RPM of the turbine. The experimental power and equivalent coefficient of power C_p are portrayed in fig.14.

Finally, the experimental and theoretical coefficient of power C_p of the scaled-down blade is compared in fig.15. The variation in the C_p for the scaled-down blade achieved through BEM shows a finite non-zero value when the turbine operates at $TSR=1$. With increase in TSR, the coefficient of power C_p slowly rises. The curve increases and lodges a maximum $C_p=0.4143$ when the TSR is 7. Beyond $TSR=7$, the curve begins experiencing a steady and restrained downfall that is not characterized by any sudden loss of power. On the other hand, the figure also shows the nature of C_p acquired experimentally. Contrary to the iterative prediction, the experimental behavior initially registers $C_p=0$ at $TSR=1$ and 2. This can be regarded to the non-origination of torque and power at speeds less than the cut-in speeds of the turbine. The turbine indexes a positive finite C_p only when the curve exceeds $TSR=3$. As the wind velocity is increased gradually, the power generated by the turbine increases and so the C_p . This incremental curve continues to rise up to $TSR=5$ is reached. Notwithstanding, the slope of the C_p begins to slow down when the wind speed is increased beyond $TSR=6$. From $TSR=6$ to $TSR=7$, the C_p curve almost remains flat with maximum value of C_p recorded at $TSR=7$. At $TSR=7$, the blade portrayed a highest C_p of 0.387. Unmistakably both the curves exhibit their best C_p precisely at $TSR=7$. But, the C_p of the scaled-down model is measured to be 0.387 which is around 6.5% less compared to the analytical C_p . The loss of C_p at $TSR=7$ may be attributed to the losses arising due to 3 Dimensional effects, unsteady aerodynamics, hub losses etc. that are not accounted in the BEM theoretical calculations. Furthermore, as the TSR is increased, the blades experience a decrement in C_p which

continues till $\lambda=12$ is reached. Beyond $TSR=12$, C_p curve presents a fall in the trend thus experiencing a loss in power.

8. Conclusions

Analytically and experimentally evaluating the performance of a 2kW small scale wind turbine rotor blade for has been presented. Blade element momentum has been utilized for designing and ascertaining the performance of the blade at operating conditions. For logistic and economic reasons the designed blade has been downsized and retrofitted to an existing wind turbine test rig through scaling laws and subsequently tested for its performance at design conditions. The major conclusions of the current research work are summarized below:

- The geometrical blade derivatives obtained through iterative BEM schema manifests large chord and twist distributions that render the blade a complex geometry. Blades exhibiting complex profiles invite special manufacturing techniques thus escalating production costs. Nevertheless, incorporation of linearization technique aids in rendering a smooth and simple blade profile that ultimately helps in reducing the manufacturing costs of the blade. Besides, the power produced by the linearized blade is just 1.8% lesser compared to the optimized blade and this difference in power output is deemed insignificant under the backdrop of huge manufacturing and economic benefits aided by linearization technique.

- Linearization further helps in reducing the solidity of the blades which are more suited for electrical wind turbines that characteristically requires high RPM rather than high Torque as in case of mechanical wind mills. Hence, linearization provides optimum solidity to the blades without compromising on the performance of the blade.

- The research also illustrates that by incorporating appropriate scaling laws, the experimental testing can be made less cumbersome without escalating the fabrication and instrumentation costs. Besides, scaling also allows obtaining all the vital aerodynamic results with a respectable accuracy within given economic constraints.

References

- [1] Phebe Asantewaa Owusu, Samuel Asumadu-Sarkodie, "A review of renewable energy sources, sustainability issues and climate change mitigation" Cogent Engineering (2016), 3: 1167990
- [2] Wind Technologies Market Report, U.S Department of Energy, 2017
- [3] Jae-Sung Bae, Dong-Guk Choi, Soo-Yong Lee, Cheol Yoo, Dae-jin Kim, "Preliminary Study on a Fabric-Covered Wind Turbine Blade", 4th International Conference on Renewable Energy Research and Applications, Palermo, Italy, 22-25 Nov 2015.
- [4] U. M. Choi, and K. B. Lee, F. Blaabjerg, "Power Electronics for Renewable Energy Systems: Wind Turbine and Photovoltaic Systems" 3rd International Conference on Renewable Energy Research and Applications, Milwaukee, USA, 19-22 Oct 2014.
- [5] SuHyeon Han, Hyun Woo Shin, "Policy Trends of Renewable Energy in Korea" 3rd International Conference on Renewable Energy Research and Applications, Milwaukee, USA, 19-22 Oct 2014.
- [6] Global Wind Energy Council, Global Wind Statistics, 2017
- [7] Environmental and Energy Study Institute, Fact Sheet, Small Scale Wind Power for Homes, Farms and Communities, July 2012.
- [8] United Nations Conference of Trade and Development (UNCTAD), Renewable Energy Technologies for Rural Development, 2010.
- [9] Taichiro Sakagami, Yu Shimizu, Hiroaki Kitano, "Exchangeable Batteries for Micro EVs and Renewable Energy" 6th International Conference on Renewable Energy Research and Applications, San Diego, CA, USA, Nov. 5-8 2017
- [10] A Dolara, A Gandelli, F. Grimaccia, S. Leva, F Mussetta, "Weather Based Machine Learning Technique for Day-Ahead Wind Power Forecasting" 6th International Conference on Renewable Energy Research and Applications, San Diego, CA, USA, Nov. 5-8 2017
- [11] Devashish, Amarnath Thakur, "A Comprehensive Review on Wind Energy System for Electric Power Generation: Current Situation and Improved Technologies to Realize Future Development" International Journal of Renewable Energy Research, Vol.7, No.4, 2017
- [12] Ronit K. Singh, M. Rafiuddin Ahmed, Mohammad Asid Zullah, Young-Ho Lee, "Design of a low Reynolds number airfoil for small horizontal axis wind turbines", Renewable Energy 42, pp. 66-76, 2012.
- [13] D.M. Somers, The S822 and S823 Airfoils, NREL/SR-500-36342.
- [14] Prasad, Navin, S. Janakiram, T. Prabu, S. Sivasubramaniam. "Design and development of horizontal small wind turbine blade for low wind speeds" International Journal of Engineering Science & Advanced Technology, Volume-4, Issue-1, 075-084, ISSN: 2250-3676, 2014.
- [15] Göçmen, Tuhfe, and Barış Özerdem. "Airfoil optimization for noise emission problem and aerodynamic performance criterion on small scale wind turbines" Energy 46, no. 1 62-71, 2012.
- [16] Somers, D. M., and M. D. Maughmer, "Theoretical Aerodynamic Analyses of Six Airfoils for Use on Small Wind Turbines" National Renewable Energy Lab (NREL), Golden, CO (United States), No: NREL/SR-500-33295, 2003 July 11, 2002-October 31, 2002.
- [17] Haibo Jiang, Yanru Li, Zhongqing Cheng, "Performances of ideal wind turbine" Renewable Energy 83 66-76, 2015.

- [18] Gur, Ohad, Aviv Rosen. "Optimal design of horizontal axis wind turbine blades" ASME 2008 9th Biennial Conference on Engineering Systems Design and Analysis, American Society of Mechanical Engineers, pp. 99-109, 2008.
- [19] Lin Wang, Xinzi Tang, and Xiongwei Liu, "Blade Design Optimisation for Fixed-Pitch Fixed-Speed Wind Turbines" International Scholarly Research Network, ISRN Renewable Energy, Volume 2012, Article ID 682859, 8 pages, doi:10.5402/2012/682859, August 2012.
- [20] P. Giguère and M.S. Selig, "Design of a Tapered and Twisted Blade for the NREL Combined Experiment Rotor", NREL/SR-500-26173, April 1999.
- [21] Pathike, Paramet, Thanad Katpradit, Pradit Terdtoon, Phrut Sakulchangsatjatai. "A new design of blade for small horizontal-axis wind turbine with low wind speed operation" Energy Research Journal Volume 4, Issue 1, Pages 1-7, DOI: 10.3844/erjsp.2013.1.7, 2013.
- [22] Collocutt, G. R., and R. G. J. Flay. "The economic optimisation of horizontal axis wind turbine design" Journal of wind engineering and industrial aerodynamics 61, no. 1:87-97, 1996.
- [23] Chaudhary, Umesh, and Sisir Kumar Nayak. "Micro and small-scale HAWT blades airfoils study through CFD for low wind applications" Annual IEEE India Conference (INDICON), pp. 1-6. IEEE, 2015.
- [24] Dixon P. Drumheller, Genevieve C. D'Antonio, Blake A. Chapman, Corey P. Allison, Olga Pierrakos, "Design of a Micro-Wind Turbine for Implementation in Low Wind Speed Environments" IEEE Systems and Information Engineering Design Symposium, 24-24 April 2015, DOI:10.1109/SIEDS.2015.7116959.
- [25] Bayati, Ilmas, Marco Belloli, Luca Bernini, Alberto Zasso. "Aerodynamic design methodology for wind tunnel tests of wind turbine rotors" Journal of Wind Engineering and Industrial Aerodynamics, 167:217-227, 2017.
- [26] Van Treuren, Kenneth W., Jason R. Gregg. "Testing of Rotating Horizontal Axis Wind Turbine Blade Designs in a Laboratory Wind Tunnel" American Society of Mechanical Engineers, In ASME Turbo Expo 2010: Power for Land, Sea, and Air, pp. 901-909, 2010.
- [27] Van Treuren, K. W., and Hays, A. W., 2017, "Understanding, Designing, and Initial Testing of Small-Scale Horizontal Axis Wind Turbines for the Urban Environment," Proceedings of the 1st Global Power and Propulsion Forum, Jan 16-18, 2017.
- [28] Bottasso, Carlo L., Filippo Campagnolo, Vlaho Petrović. "Wind tunnel testing of scaled wind turbine models: Beyond aerodynamics" Journal of wind engineering and industrial aerodynamics 127:11-28, 2014.
- [29] Miguel Toledo Velázquez, Marcelino Vega Del Carmen, Juan Abugaber Francis, Luis A. Moreno Pacheco, Guilbaldo Tolentino Eslava, "Design and Experimentation of a 1 MW Horizontal Axis Wind Turbine" Journal of Power and Energy Engineering, 2014, 2, 9-16.
- [30] Xiongwei Liu, Lin Wang, Xinzi Tang, "Optimized linearization of chord and twist angle profiles for fixed-pitch fixed-speed wind turbine blades", Renewable Energy 57 (2013) 111-119.